Supplementary Information

Synergy of Organoiodide Additives and Co-Solvent Enabling High-Performance Wide-Temperature Zn Metal Batteries

Xin Miao[+1], Jingjing Bao[+1], Shuang Li[+1], Changjun He[1], Ziyang Guo[1], Yonggang Wang*[1,2]*

[1] College of Energy Material and Chemistry, College of Chemistry and Chemical Engineering, Inner Mongolia University, Hohhot, China.

[2] Department of Chemistry and Shanghai Key Laboratory of Molecular Catalysis and Innovative Materials, Institute of New Energy, iChEM (Collaborative Innovation Center of Chemistry for Energy Materials), Fudan University, Shanghai, China.

[+] These authors contributed equally to this work.

Corresponding authors

*Ziyang Guo (E-mail: zyguo@imu.edu.cn); Yonggang Wang (E-mail: ygwang@fudan.edu.cn)

Materials and Methods

Materials: Ketjen Black EC-600JD (KB), polytetrafluoroethylene (PTFE) (solid content 60%), Zinc foil (10, 30 and 100 μm, 99.99%), copper foil (20 μm), titanium foil (20 μm), titanium steel, and coin cells (CR2016) were all purchased from the Canrd company. Glass fiber separator (GF/D) was purchased from Whatman. Zinc trifluoromethanesulfonate (> 98%), Isopropanol (99.9%), Tetrahydrofuran (99.0%) were obtained from the Innochem. Vanadium pentoxide (≥ 99.99% metals basis) was purchased from Aladdin, Sodium chloride (NaCl, 99.99%) was purchased from Macklin, Triethylsulfonium Iodide (97%) was purchased from Yuan Ye. All chemicals were used as received without further purification.

Preparation of $NaV_3O_8 \cdot 1.5\ H_2O$ (NVO): 1 g of commercial V_2O_5 powder was dispersed into 15 mL of an aqueous solution containing 2 M NaCl. After continuous stirring for 96 h at 30 °C, the suspension was washed with deionized water and ethanol several times. Finally, the $NaV_3O_8 \cdot 1.5H_2O$ product was obtained by overnight drying in the air at 60 °C.

Fabrication of the NVO electrodes and assembly of the corresponding full/half cells: The cathode material was prepared by mixing NVO powder, KB, and polytetrafluoroethylene (PTFE) in a mass ratio of 7:2:1 with an appropriate amount of isopropanol to form a paste. The paste was then rolled into a thin film and pressed onto a titanium mesh. The Ti mesh coated with cathode material was vacuum-dried at 80 °C for the whole night before being punched or cut into different-shaped NVO cathodes for battery assembly. The mass loading of the active material in the coin cells ranged from 3.0 to 15.3 mg cm^{-2}. The commercial Zn foil with a thickness of 100 μm was polished using an abrasive paper to remove the passivation layer, washed with ethanol, and dried. The polished Zn foil was then

cut into 12 mm diameter discs, which were used as the Zn anode for the Zn//Zn symmetric cells, the Zn//Ti asymmetric cells, and the Zn//NVO full cells. The electrolyte volume for each cell was kept to a maximum of 100 μL.

Fabrication and testing of the pouch cells: Firstly, the pouch cells were fabricated using NVO electrodes (working area: 4 × 3 cm^2 or 4 × 7 cm^2, mass loading: 4.33 or 32.6 mg cm^{-2}, Ti mesh current collector) as cathodes, Zn foils (working area: 4.2 × 3.2 cm or 4.2 × 7.2 cm^2, 100 or 30 μm thick) as anodes, and T50+TSI (the electrolyte dosage: 0.1 or 0.06 mL cm^{-2}) as electrolyte. The cells were subsequently encapsulated and sealed within an aluminum plastic film. After that, the cycling performance and galvanostatic charge-discharge tests of the obtained pouch cells were conducted on Neware CT4008Tn (Shenzhen, China) battery test systems.

Electrochemical measurements: All batteries were assembled in an open environment and aged for 0.5 h before electrochemical measurements. Their electrochemical performances were tested in CR2016-type coin cells using LAND (LAND-CT3002A) battery testing system. To evaluate the coulombic efficiency (CE) with the cut-off potential of 0.8 V, the Zn//Ti cells were assembled. The cycling performance and rate capability of the Zn//NVO full cells were tested between the voltages of 0.2 V~1.2 V. In the RDEJ-100 high and low temperature test chamber, which has a working temperature range of -75 °C to 150 °C, the low-temperature battery performance was assessed. Linear scanning voltammetry (LSV) experiment was performed with a positive scan to -0.9 V and a negative scan to -1.8 V at a scan rate of 1 mV s^{-1}, respectively. The chronoamperometry curve (CA) of the Zn//Zn cell was obtained at a fixed overpotential of -150 mV. The electrochemical impedance spectra (EIS) were measured of the Zn//Zn cells in a frequency range from 10 kHz to 0.1 Hz with a voltage amplitude of 5 mV (AUTOLAB electrochemical workstation). The ionic conductivity of different

electrolytes at 25 °C was measured using an electrochemical workstation (CHI660E). The ionic conductivity (σ) can be calculated by the following equation:

$$\sigma = \frac{L}{R * S} \qquad \text{(Equation S1)}$$

Where R represents resistance according to the EIS measurement, L represents the thickness of the electrolyte, and S is the contact area between the electrode and electrolyte in the testing cell. The galvanostatic charge/discharge (GCD) measurements were performed by a battery test system (LAND 3002A). The cycle life and coulombic efficiency were also tested by the battery test system.

The activation energy during Zn^{2+} deposition was calculated according to the following Arrhenius equation (2):

$$k = \frac{T}{R_{\text{res}}} = A exp\,(-\frac{E_{\text{a}}}{RT}) \qquad \text{(Equation S2)}$$

where k is the rate constant; T (K) is absolute temperature; R_{res} (Ω) is ion transfer resistance; A is the preexponential constant; E_a (kJ mol^{-1}) is the activation energy; and R (8.314 $J \cdot mol^{-1} \cdot K^{-1}$) is the standard gas constant. The Zn//Zn symmetric were assembled and put in the temperature chamber for 20 min before tests.

***In-situ* Raman measurements:** The Zn plating/stripping behaviors of the symmetric cells with T0 or T50+TSI were monitored under a current density of 2 mA cm^{-2} with the fixed capacity of 2 mAh cm^{-2} by an *in-situ* Raman spectroscopy (Horiba LabRAM HR Evolution, HORIBA FRANCE SAS, France), combining with a LAND battery testing system (LAND-CT3002A, Wuhan). The Raman laser was focused on the local Zn electrode at the bottom, with a spectra center of 2300.00 cm^{-1}, a laser

wavelength of 532 nm, a laser intensity of 10.00, and 2 single spectra per 120 seconds.

***In-situ* optical microscope:** For *in-situ* optical microscopy measurements, a customized cell was utilized. Two Zn foils were fixed parallelly with a gap between them, followed by the introduction of the electrolyte. The entire assembly was then mounted under an *in-situ* optical microscope (Model YM710R) to observe the Zn deposition behavior during plating. Simultaneously, it was connected to a LAND test system for the electrochemical test.

Alternating current voltammetry (ACV) test: Firstly, the Zn//Ti batteries were constructed by using Zn foils as anodes, Ti foils as cathodes and T0, T50 or T50+TSI as electrolytes, respectively. Subsequently, the assembled Zn//Ti cells were connected with a CHI 660E electrochemical workstation. During the electrochemical tests, the frequency and amplitude were set to 6 Hz and 0.005 V, respectively, with a scanning window from 1 V to -0.1 V and a scan rate of 4 mV s^{-1}. Finally, the acquired data was directly used for analysis.

Materials Characterization: The freezing point was tested by differential scanning calorimetry (DSC) through American TA Q2000. The sealed aluminum pan with about 10 mg of electrolyte was cooled from room temperature to -80 °C, holding isothermally for 20 min, and then heated until 20 °C with a rate of 5°C·min^{-1} under nitrogen atmosphere. The comparison of the contact angles between different electrolytes and Zn substrate was recorded using the sessile drop contact angle technique (PZ-350SD, Pinzhichuangsi Co., Ltd). The morphologies of the electrodes and the corresponding elemental analysis were observed using field emission scanning electron microscopy (SEM, TESCAN MIRA LMS, Czech). The crystalline structure of the electrodes was characterized by X-ray diffraction (XRD, Bruker D8 Advance diffractometer, Cu Kα radiation, Scan rate: 10° min^{-1}) over a range of 5° to 80°. The elemental composition was determined by X-ray photoelectron spectroscopy (XPS,

ESCALAB 250xi, Thermo Fisher Scientific). Attenuated total reflection Fourier transform infrared spectroscopy (ATR-FTIR, SHIMADZU, IRAffinity-1s) analysis was carried out spectroscopy from 400 to 4000 cm^{-1} with a resolution of 4 cm^{-1} and averaging 64 scans for each spectrum. H magnetic resonance imaging (NMR spectroscopy (Bruker 600 MHz).

Theoretical Calculations: The calculations about HOMO and LUMO energies were carried out with the Gaussian 09 package. Geometry optimizations were performed with B3LYP method. The 6-31+G (d, p) basis set was used for all atoms. The calculations about interaction energies between small molecules and Bader charges were performed with the Vienna ab initio simulation package (VASP), using the Perdew-Burke-Ernzerhof (PBE) exchange-correlation functional was depicted through a plane wave with an energy cutoff of 400 eV to ensure the precision of the calculations. For calculations of geometries, the integrations over the Brillouin zone were performed with a 1×1×1 special k-point mesh. The convergence criterion for the electronic self-consistent cycle was controlled at 0.01 eV per cell. The geometry optimization was stopped when the forces on all unconstrained atoms were less than 0.05 eV $Å^{-1}$.

Figures and Tables

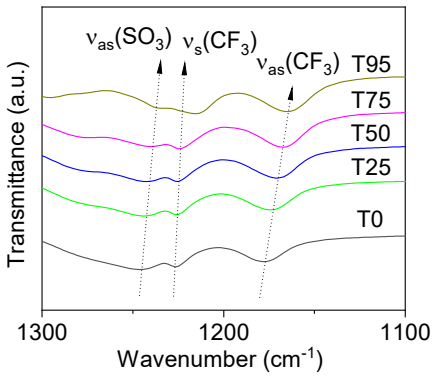

Figure S1. FT-IR spectra for the hybrid electrolytes with different volume ratios between H_2O and THF.

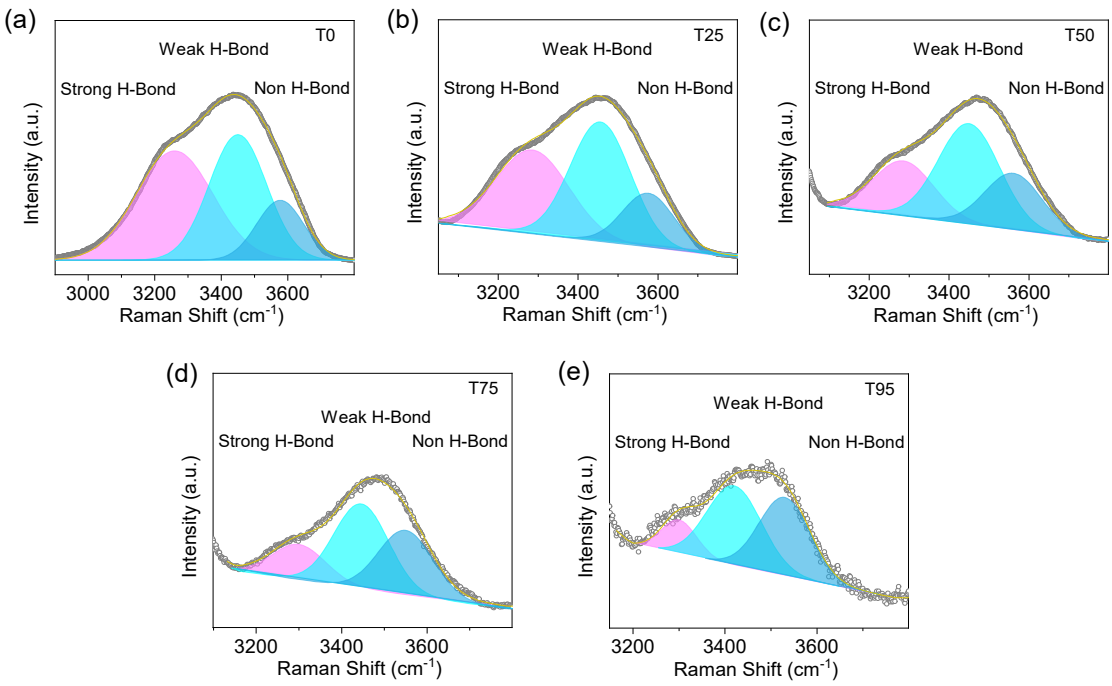

Figure S2. Fitting deconvolution of Raman spectra for the hybrid electrolytes with different volume ratios between H_2O and THF.

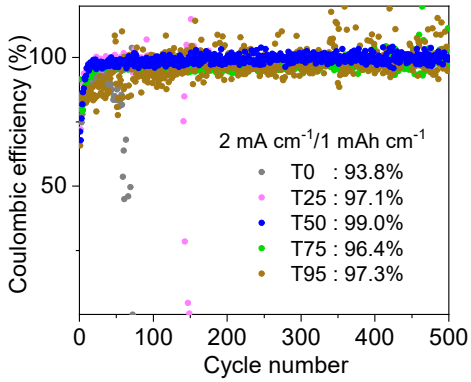

Figure S3. The Coulombic efficiencies (CEs) of the Zn//Ti half-cells with T0, T25, T50, T75 or T95.

As shown in **Figure S3**, when the contents of THF in the hybrid electrolytes are very low (e.g. T0 and T25), the CEs of the corresponding half-cells display the significant fluctuations from the initial cycles. This indicates that the limited introduction of THF cannot effectively suppress the highly active H_2O-induced hydrogen evolution reaction (HER) or other side reactions and thus leads to the serious reversibility in these cells.[1, 2] When the contents of THF in the hybrid electrolytes are very high (e. g. T95 and T75), the CEs of the corresponding half-cells also present the obvious fluctuations over cycling which may be mainly originated from the non-uniform Zn deposition. Specifically, although the high THF contents in the hybrid electrolytes suppress the water-induced side reactions, their low dielectric constant reduces the ionic conductivity and increases the de-solvation energy barrier of the hybrid electrolytes, resulting in the localized zinc deposition into the dendritic or mossy structures and the formation of dead Zn. These finally lead to the notable reversible capacity loss and CE instability.[3, 4] In comparison, the T50-based Zn//Ti half-cell with an appropriate THF ratio not only effectively suppresses water-induced side reactions such as HER, but also guides the uniform Zn deposition. Therefore, the T50-based battery shows the relatively stable and high CEs over the whole cycling.

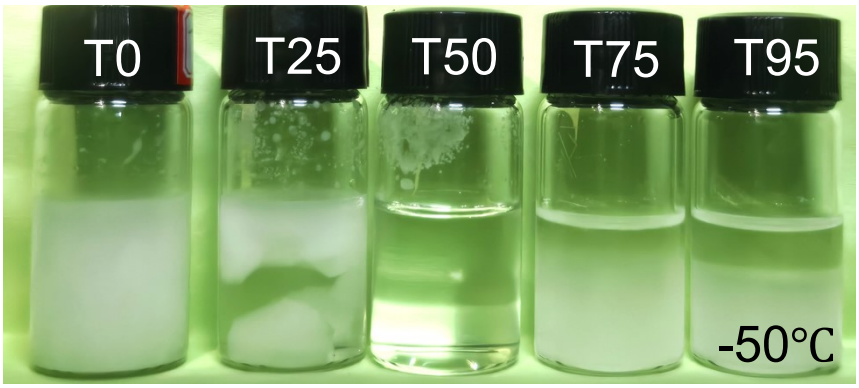

Figure S4. The freezing behaviors of T0, T25, T50, T75 and T95 at -50 °C.

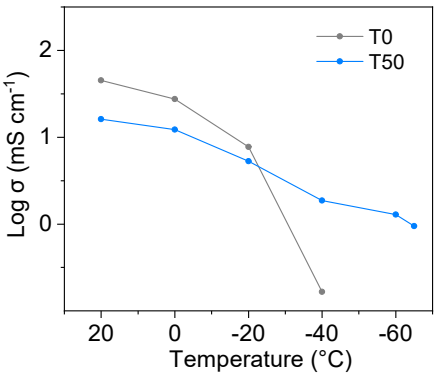

Figure S5. Ionic conductivities of T0 and T50 at different low temperatures.

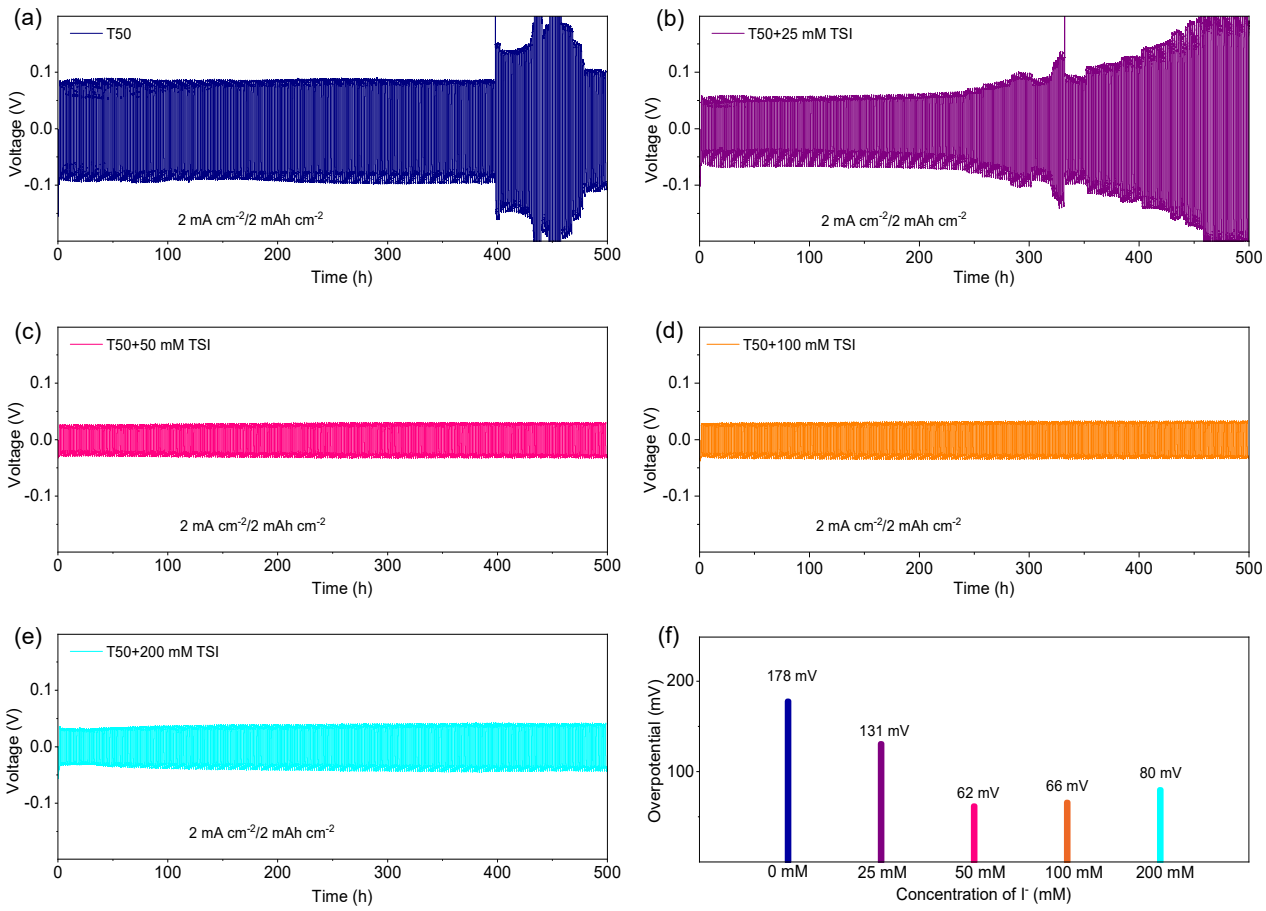

Figure S6. Polarization voltage curves of the Zn//Zn symmetric cells using T50+TSI with different TSI additive amounts under 2.0 mA cm^{-2} with limited capacity of 2.0 mAh cm^{-2}.

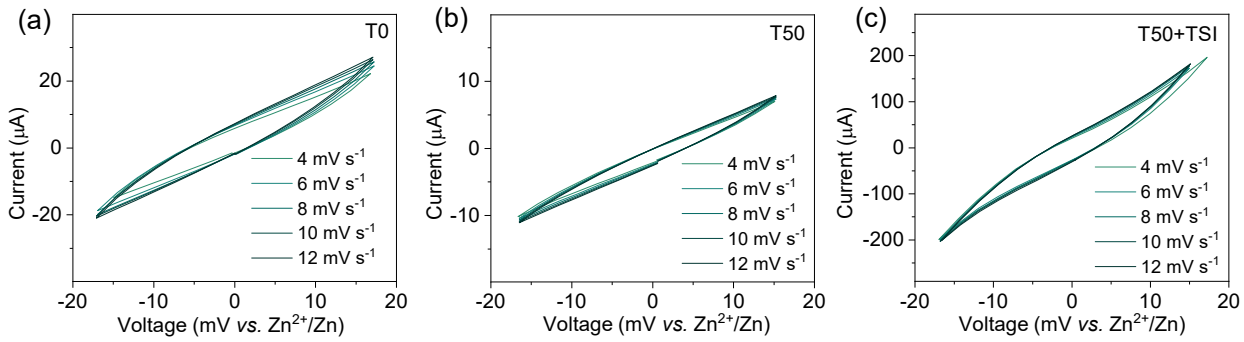

Figure S7. Cyclic voltammetry (CV) curves for the Zn//Zn cells with (a) T0, (b) T50 or (c) T50+TSI.

The electric double layer (EDL) capacitances (C, mF cm^{-2}) are determined through cyclic voltammetry (CV) measurements conducted on the Zn//Zn symmetric cells with varying electrolytes at multiple scan rates. These capacitance values at 0 V *vs.* Zn/Zn^{2+} were quantified using the fundamental capacitance relationship $C = i/v$, where i corresponds to the measured current density and v denotes the applied voltage scan rate.

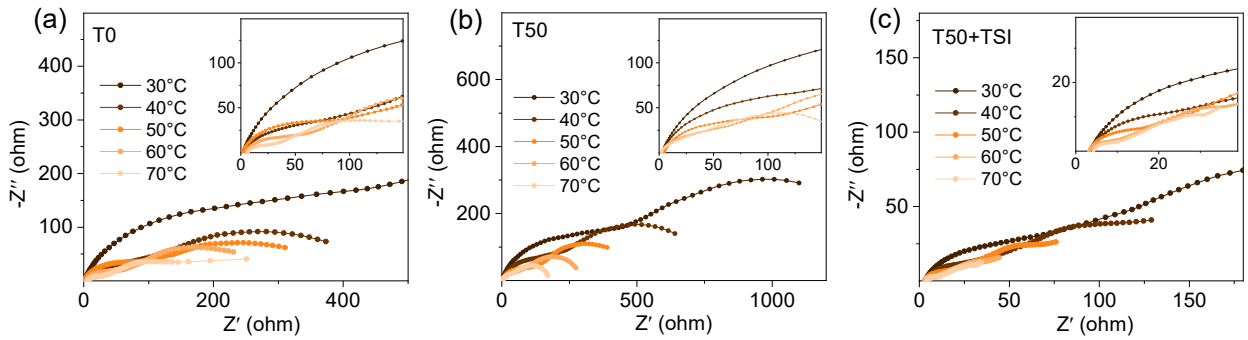

Figure S8. EIS measurements of the symmetric cells with (a) T0, (b) T50 or (c) T50+TSI under different temperatures.

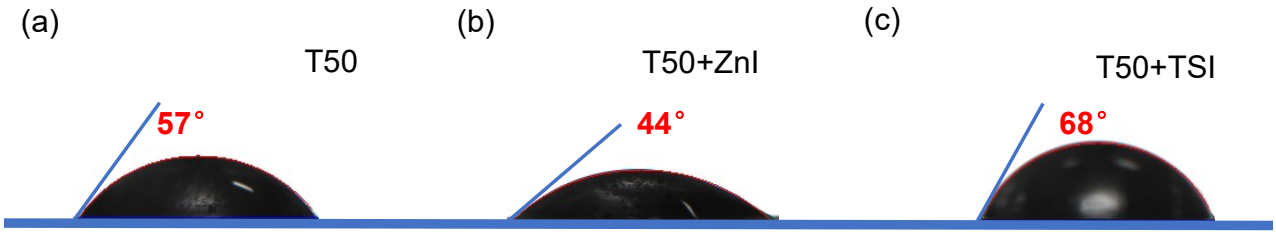

Figure S9. The contact angles of water with Zn sheets that were pretreated with different electrolytes: (a) T50, (b) T50+ZnI and (c) T50+TSI. (where T50+ZnI is 50% volume of THF and H_2O+50 mM ZnI).

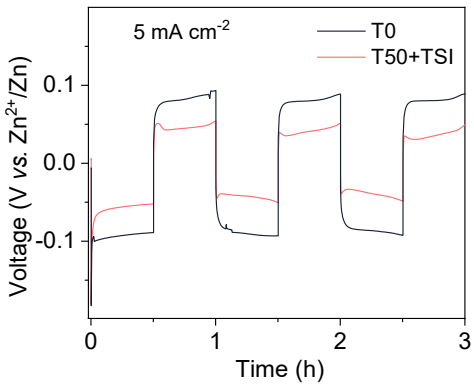

Figure S10. Time-voltage profiles of the symmetric cells with T0 or T50+TSI at 5.0 mA cm^{-2} with an area capacity of 2.5 mAh cm^{-2} during *in-situ* differential electrochemical mass spectrometry (DEMS) testing.

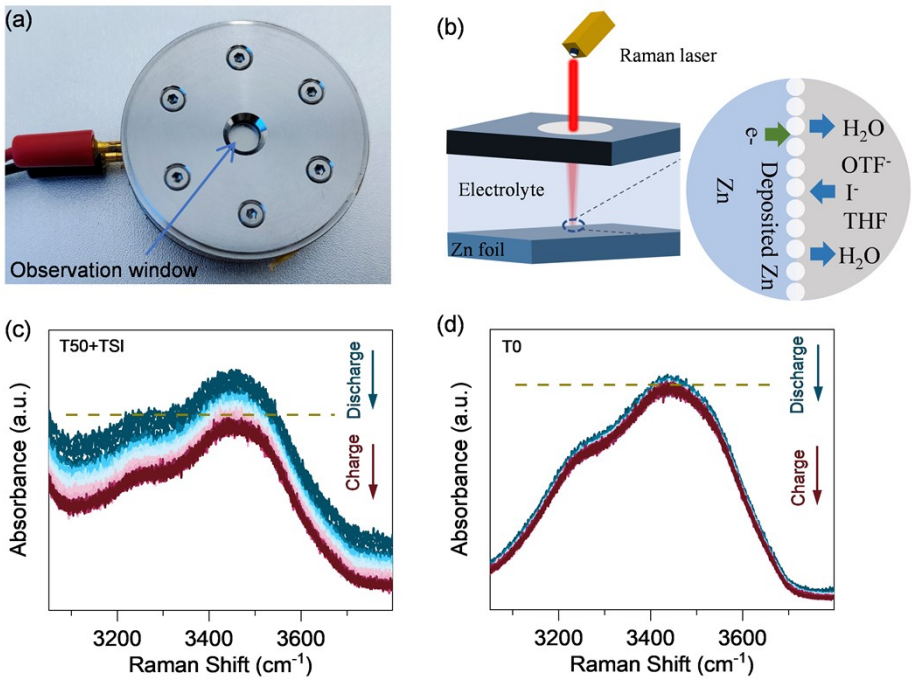

Figure S11. (a) Photograph and (b) schematic diagram of the customized battery for the *in-situ* Raman measurements. *In-situ* Raman spectra curves at the interfaces of the Zn anodes under different discharge/charge conditions in the symmetric cells using (c) T50+TSI or (d) T0.

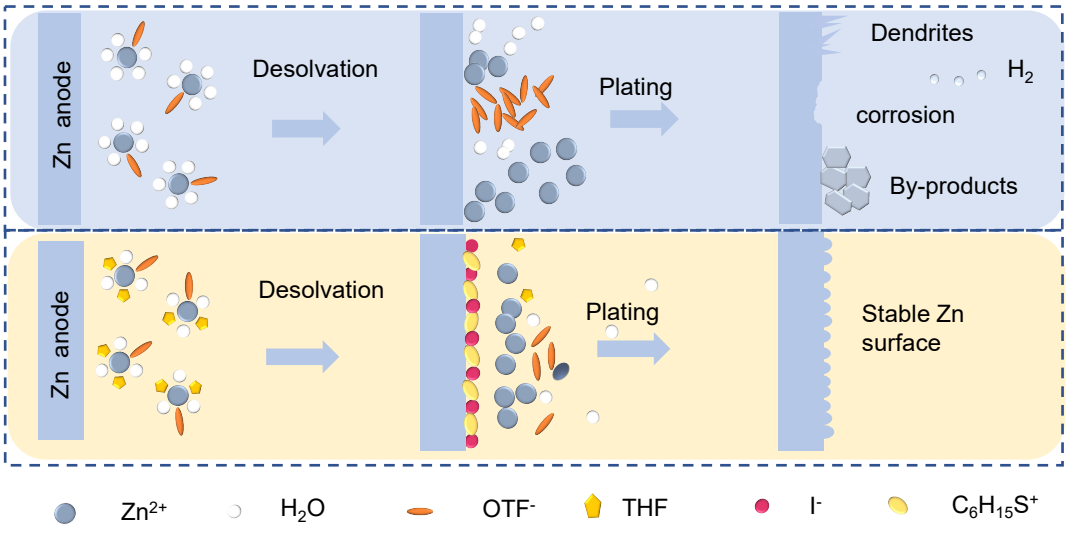

Figure S12. The schematic diagrams of the interface variations between Zn anodes in T0 or T50 +TSI over charging.

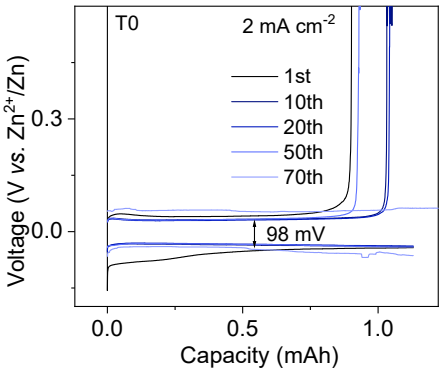

Figure S13. The corresponding voltage profiles of the Zn//Ti cell using T0.

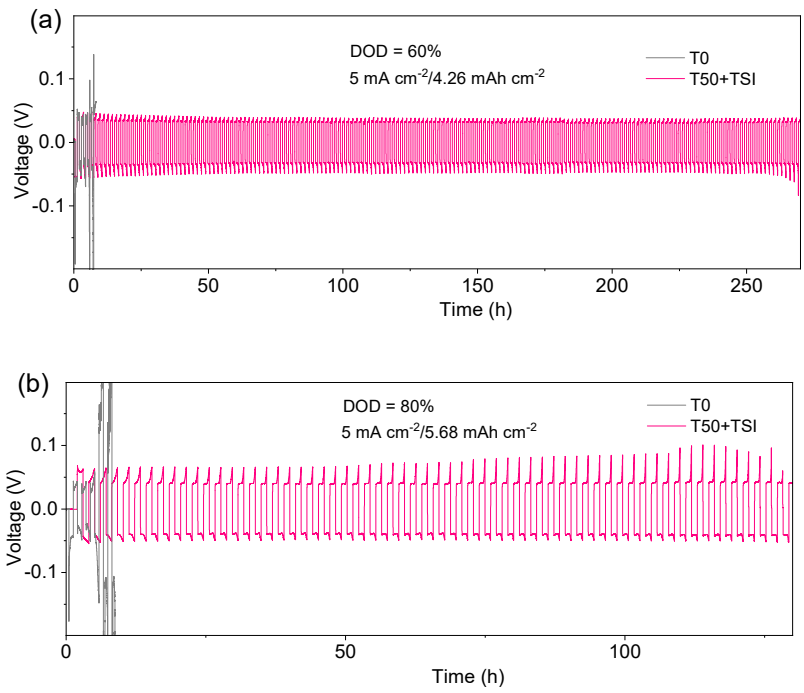

Figure S14. The cycling performances of the Zn//Zn cells with a DOD of (a) 60 % and (b) 80 % in T0 or T50+TSI.

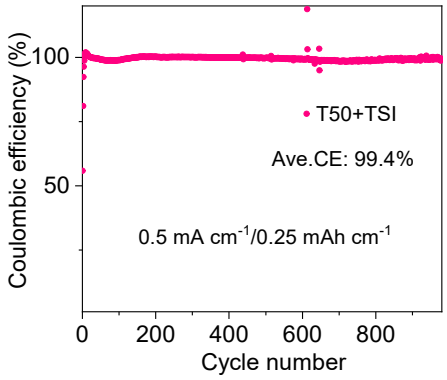

Figure S15. The CE of the Zn//Ti cell with T50+TSI at -30 °C.

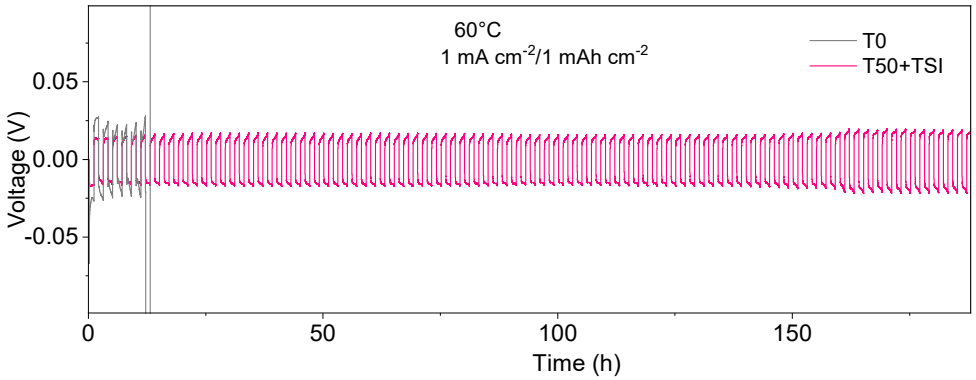

Figure S16. The continuous discharge/charge profiles of the Zn//Zn cells using T50+TSI or T0 under 60 °C at 1 mA cm^{-2} with the fixed capacity of 1 mAh cm^{-2}.

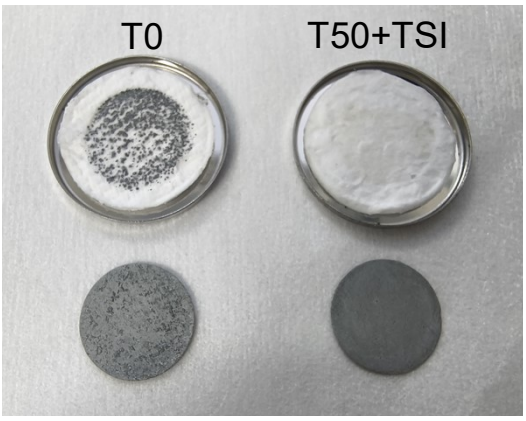

Figure S17. Digital photograph of the cycled Zn anodes and corresponding glass fiber films in T0 or T50+TSI at the current density of 2.0 mA cm^{-2} with the fixed capacity of 2.0 mAh cm^{-2}.

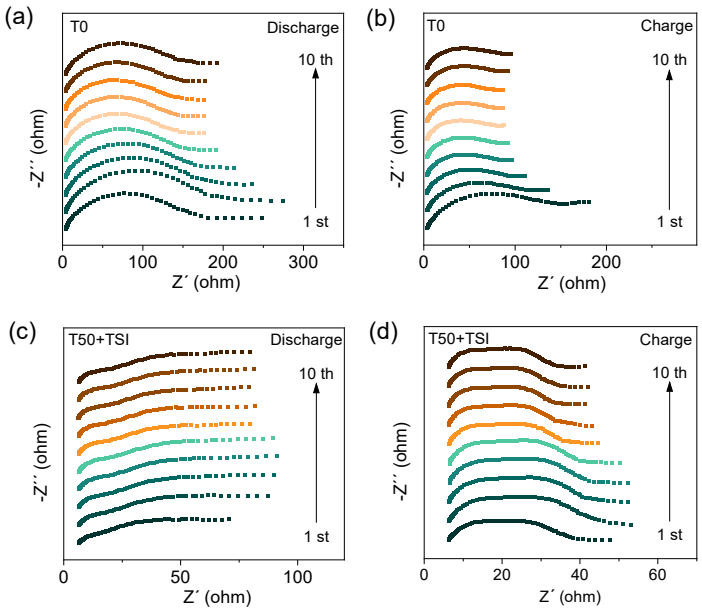

Figure S18. *In-situ* EIS data of the symmetrical batteries at various cycles during Zn plating with (a) T0 or (c) T50+TSI. *In-situ* EIS data of the symmetrical batteries at various cycles during Zn stripping with (b) T0 or (d) T50+TSI.

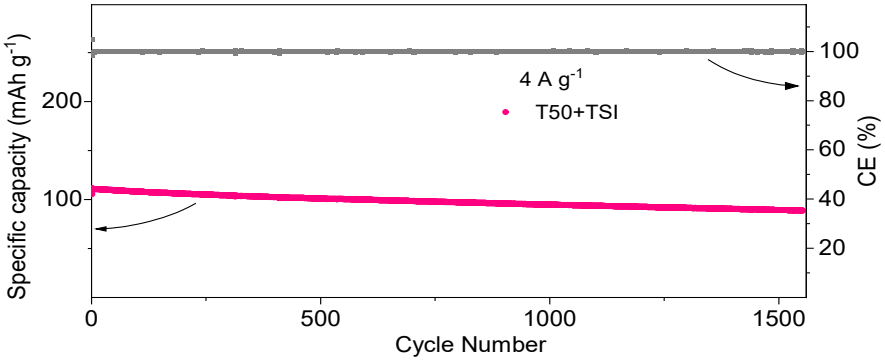

Figure S19. Cycling performance of the Zn//NVO full cell using T50+TSI at a high current density of 4 A g^{-1} under room temperature.

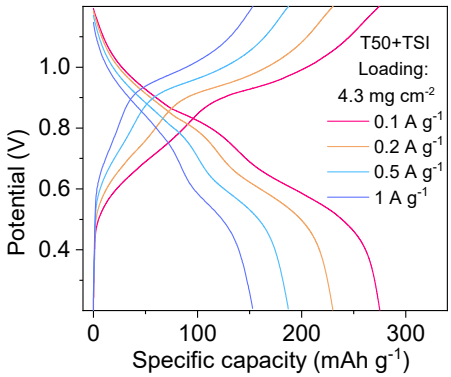

Figure S20. Charge/discharge curves of the Zn//NVO full cell with the cathode mass-loading of 4.3 mg cm^{-2} at different currents.

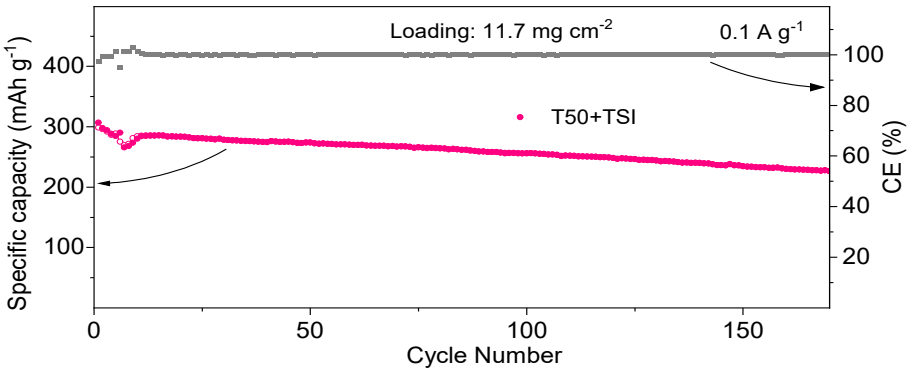

Figure S21. The cycling performance of the NVO cathode with the mass-loading of 11.7 mg cm^{-2} in T50+TSI at 100 mA g^{-1}.

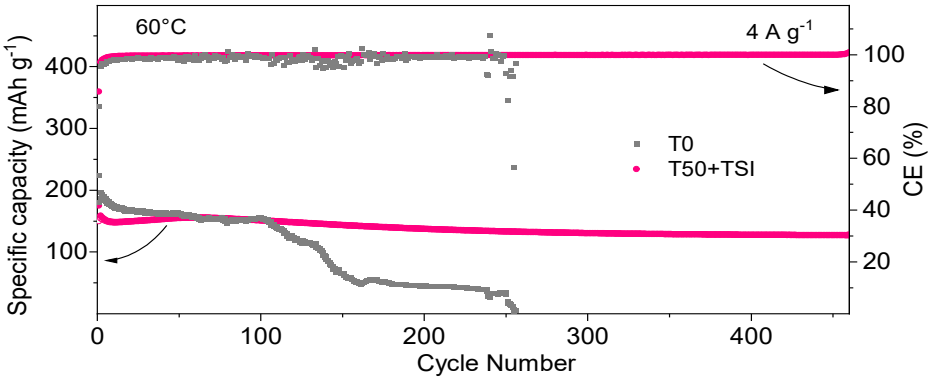

Figure S22. Cycling performances of the Zn//NVO full batteries with T50+TSI or T0 under 60 °C at 4 A g^{-1}.

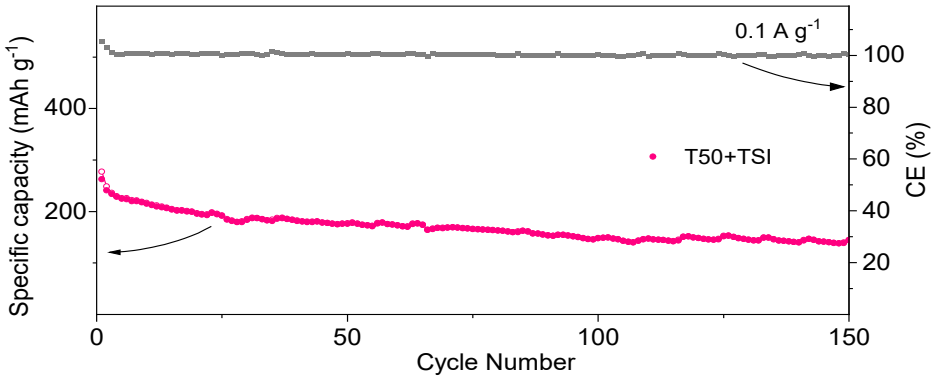

Figure S23. Cycling performance of the Zn//NVO pouch cell in T50+TSI at 100 mA g^{-1} under room temperature.

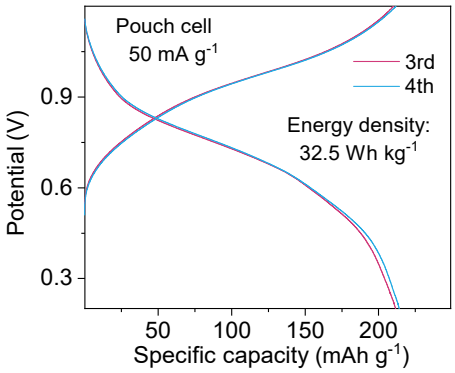

Figure S24. The galvanostatic charge/discharge profiles of the Zn//NVO pouch cell with high mass-loading cathode at the current density of 50 mA g^{-1} and its energy density based on the total weight of the cathode, anode and electrolyte (4.2 g).

Table S1. Equivalent circuit model (ECM) and corresponding fitting data of *in-situ* EIS spectra of the Zn//Zn symmetric cells with T0 or T50+TSI during the discharge process.

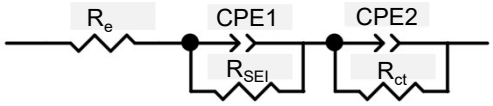

NO	T0		T50+TSI	
	R_{ct} (Ω)	Error (%)	R_{ct} (Ω)	Error (%)
1	471.0	7.03	77.1	7.26
5	402.8	8.47	91.0	7.71
10	327.3	6.28	84.4	7.91
15	266.5	4.83	73.4	6.60
18	236.2	4.00	68.6	6.19

Table S2. Comparison of the electrochemical performances of the T50+TSI-based Zn//Zn cell in this work and the previously reported Zn//Zn cells with co-solvent-based hybrid electrolytes.

NO	Electrolyte	Current density	Capacity plated (mAh cm^{-2})	Cycle life (h)	Ref.
1	2 M $Zn(OTF)_2$ + 50 vol.% THF + 50 vol.% H_2O + 50 mM TSI	2 mA cm^{-2}/2 mAh cm^{-2}	7.1	7100	This work
2	1 M $Zn(OTF)_2$ + 50 vol.% H_2O + 50 vol.% PC	1 mA cm^{-2}/0.5 mAh cm^{-2}	1.6	1600	[1]
3	1 M $Zn(OTF)_2$ + 60 vol.% H_2O + 40 vol.% TPP	1 mA cm^{-2}/1 mAh cm^{-2}	1.5	3000	[5]
4	1 M $Zn(OAc)_2$+50 vol.% H_2O + 50 vol.% FA	0.5 mA cm^{-2}/0.25 mAh cm^{-2}	0.43	860	[6]
5	1 M $Zn(OTF)_2$ + 50 vol.% DMAC + 20 vol.% TMP + 30 vol.% H_2O	1 mA cm^{-2}/1 mAh cm^{-2}	1.6	3200	[7]
6	2 M $Zn(ClO_4)_2$ + BDO/H_2O（x_{BDO}=0.27)	1 mA cm^{-2}/1 mAh cm^{-2}	0.9	1800	[8]
7	2 M $Zn(OTF)_2$ + 70 vol.% H_2O + 30 vol.% CPME	2 mA cm^{-2}/2 mAh cm^{-2}	2.4	2400	[9]
9	2 M $Zn(OTF)_2$ + 80 vol.% H_2O + 20 vol.% TMU	1 mA cm^{-2}/1 mAh cm^{-2}	1.65	3300	[10]
10	2 M $Zn(OTF)_2$ + 80 vol.% H_2O + 20 vol.% HMPA	1 mA cm^{-2}/1 mAh cm^{-2}	2.6	5200	[11]
12	2 M $ZnSO_4$ + 90 vol.% H_2O + 10 vol.% TMP	1 mA cm^{-2}/1 mAh cm^{-2}	1.4	2800	[12]
13	3 M $Zn(OTF)_2$ + 70 vol.% H_2O + 30 vol.% DMPU	2 mA cm^{-2}/2 mAh cm^{-2}	2.76	2760	[13]
14	1 M $Zn(OTF)_2$ + 40 vol.% H_2O + 60 vol.%PM + 0.05 M ZnI_2	0.2 mA cm^{-2}/2 mAh cm^{-2}	0.016	1650	[14]
15	0.5 M $Zn(OTF)_2$ + 70 vol.% H_2O + 30 vol.% THF	1 mA cm^{-2}/1 mAh cm^{-2}	1.4	2800	[15]
16	1 M $Zn(TFSI)_2$ + 50 mol.% H_2O + 50 mol.% Sulfolane	1 mA cm^{-2}/1 mAh cm^{-2}	4.8	9600	[16]
17	1 M $Zn(TFSI)_2$ + 20wt%H_2O + 80wt%DMSO + 0.5 m FF	1 mA cm^{-2}/1 mAh cm^{-2}	2.75	5500	[17]

Abbreviation Notes:

Tripropyl phosphate (TPP)

Dimethylacetamide (DMAC)

Cyclopentyl methyl ether (CPME)

Tetrahydrofuran (THF)

1,3-butanediol (BDO)

Propylene glycol methyl ether (PM)

Propylene carbonate (PC)

Formamide (FA)

Trimethyl phosphate (TMP)

Tetramethylurea (TMU)

N, N-Dimethylpropyleneurea (DMPU)

Hexamethylphosphoramide (HMPA)

Trifluoroethyl formate (FF)

Table S3. Comparison of the electrochemical performances of the T50+TSI-based Zn//Zn cell in this work and the previously reported Zn//Zn cells with co-solvent-based hybrid electrolytes operating at the low temperature range.

NO.	Electrolyte	Current density	Temperature (°C)	Cycle life (h)	Ref.
1	2 M $Zn(OTF)_2$ + 50 vol.% THF + 50 vol.% H_2O + 50 mM TSI	0.5 mA cm^{-2}/0.25 mAh cm^{-2}	-30	6400	This work
2	1 M $Zn(OAc)_2$ + 50 vol.% H_2O + 50 vol.% FA	0.5 mA cm^{-2}/0.25 mAh cm^{-2}	-40	770	[6]
3	2 M $ZnSO_4$ + 80 vol.% H_2O + 20 vol.% DMF	0.5 mA cm^{-2}/0.5 mAh cm^{-2}	-20	2000	[18]
4	2 M $Zn(OTF)_2$ + 60 vol.% H_2O + 40 vol.% DG	1 mA cm^{-2}/0.5 mAh cm^{-2}	-35	1000	[19]
5	2 M $Zn(OTF)_2$ + 75 vol.% H_2O + 25 vol.% TMU	0.5 mA cm^{-2}/0.5 mAh cm^{-2}	-30	300	[20]
6	1 M $Zn(OTF)_2$ + 60 vol.% G2 + 40 vol.% H_2O	0.1 mA cm^{-2}/0.1 mAh cm^{-2}	-45	2200	[21]
7	$Zn(OTF)_2$ + 70 vol.% H_2O + 30 vol% 2-propanol	0.5 mA cm^{-2}/0.5 mAh cm^{-2}	-40	4000	[22]
8	3 M $Zn(OTF)_2$ + 70 vol.% H_2O + 30 vol.% HFIP	1 mA cm^{-2}/1 mAh cm^{-2}	-25	1000	[23]
9	1 M $Zn(OTF)_2$ + 35 vol.% H_2O + 65 vol.% DMF	0.2 mA cm^{-2}/ 0.1 mAh cm^{-2}	-60	225	[24]
10	2 M $Zn(OTF)_2$ + 50 vol.% H_2O + 50 vol.% DMSO	0.5 mA cm^{-2}/0.5 mAh cm^{-2}	-40	2600	[25]
11	2 M $Zn(OTF)_2$ + 88 vol.% H_2O + 12 vol.% TG	1 mA cm^{-2}/1 mAh cm^{-2}	-35	400	[26]
12	1 M $Zn(OTF)_2$ + 30 vol.% H_2O + 70 vol.% THFA	0.3 mA cm^{-2}/0.15 mAh cm^{-2}	-40	1900	[27]
13	2M $Zn(ClO_4)_2$ + 60 wt.% H_2O + 40 vol.% PC	1 mA cm^{-2}/1 mAh cm^{-2}	-25	400	[28]
14	2M $Zn(OTF)_2$ + 80 vol.% H_2O + 20 vol.% γ-GVL	0.2 mA cm^{-2}/0.2 mAh cm^{-2}	-40	2300	[29]
15	1M $Zn(OTF)_2$ + 50 vol.% H_2O + 50 vol.% DOL	0.2 mA cm^{-2}/0.2 mAh cm^{-2}	-80	2000	[30]
16	2M $ZnCl_2$ + 70 wt.% H_2O + 30 wt.% PEG	0.5 mA cm^{-2}/0.5 mAh cm^{-2}	-25	520	[31]

Abbreviation Notes:

Diethylene glycol monoethyl ether (DG)
Diethylene glycol dimethyl ether (G2)
Hexafluoro-2-propanol (HFIP)
Tetrahydrofurfuryl alcohol (THFA)
1,3-dioxolane (DOL)
Polyethylene glycol (PEG)
Formamide (FA)
Tetraglyme (TG)
γ-valerolactone (γ-GVL)
N, N-Dimethylformamide (DMF)

Table S4. Comparison of the electrochemical performances of the T50+TSI-based full cell in this work and the previously reported full cells with co-solvent-based hybrid electrolytes operating at the low temperature range.

NO.	Cathode materials	Temperature (°C)	Current density	Specific capacity (mAh g^{-1})	Cycle number	Ref.
1	NVO	-30	0.1 A g^{-1}	70.6	1480	This work
2	PANI	-10	5 A g^{-1}	95	2000	[20]
3	PANI	-20	2 A g^{-1}	80	1000	[28]
4	VO_2	-20	0.5 A g^{-1}	220	300	[29]
5	I_2	-40	0.4 A g^{-1}	173.6	300	[31]
6	PANI	-40	0.1 A g^{-1}	91.21	600	[32]
7	V_2O_5	-15	0.1 A g^{-1}	90	450	[33]
8	TCBQ	-40	0.1 A g^{-1}	76.3	700	[34]
9	VO_2	-18	1 A g^{-1}	140	500	[35]
10	PANI	-30	0.5 mA cm^{-2}	80	800	[36]

Abbreviation Notes:

$NaV_3O_8 \cdot 1.5H_2O$ (NVO)

Polyaniline (PANI)

Tetrachlorobenzoquinone (TCBQ)

References

1. F. Ming, Y. Zhu, G. Huang, A.-H. Emwas, H. Liang, Y. Cui and H. N. Alshareef, *J. Am. Chem. Soc.*, 2022, **144**, 19577–19585.
2. M. Li, X. Feng, J. Yin, T. Cui, F. Li, J. Chen, Y. Lin, X. Xu, S. Ding and J. Wang, *J. Mater. Chem. A*, 2023, **11**, 25545–25554.
3. Z. Zhao, C. Tang, Y. Zhang, H. Zhang, X. Shi, H. Zhao, G. Wang, J. Liu and L. Li, *Energy Storage Mater.*, 2024, **70**, 103515.
4. L. Geng, J. Meng, X. Wang, W. Wu, K. Han, M. Huang, C. Han, L. Wu, J. Li, L. Zhou and L. Mai, *Chem*, 2025, **11**, 1–13.
5. P. Wang, Y. Zhong, J. Wang, H. Zhou, G. Sun, X. Sui and Z. Wang, *Adv. Funct. Mater.*, 2024, **35**, 2414563.
6. C. You, R. Wu, X. Yuan, L. Liu, J. Ye, L. Fu, P. Han and Y. Wu, *Energy Environ. Sci.*, 2023, **16**, 5096–5107.
7. Y. Wang, J. A. Yuwono, Z. Wang, W. K. Pang, G. Liang, S. Liu, W. Lie, A. M. D'Angelo, J. Deng and Z. Guo, *Nat. Commun.*, 2023, **14**, 2720.
8. Y. Liu, M. Qiu, Y. Liang, J. Zhang, J. Chen, P. Sun and W. Mai, *Angew. Chem., Int. Ed.*, 2025, **64**, e202506010.
9. J. Cong, Z. Hu, L. Hu, T. Li, H. Ji, Z. Long, Y. Fan, Z. Wen, Y.-C. Lin, H. Xu, Z. Li, S. Li, F. Pan and Y. Huang, *Adv. Funct. Mater.*, 2025, **35**, 2424423.
10. Z. Li, Y. Liao, Y. Wang, J. Cong, H. Ji, Z. Huang and Y. Huang, *Energy Storage Mater.*, 2023, **56**, 174–182.

11. Z. Huang, Z. Li, Y. Wang, J. Cong, X. Wu, X. Song, Y. Ma, H. Xiang and Y. Huang, *ACS Energy Lett.*, 2023, **8**, 372–380.

12. T. Zhang, J. Yang, H. Wang, H. Yu, Q. Li, L. Chen, Y. Chen and T. Wang, *Energy Storage Mater.*, 2024, **65**, 103085.

13. Y. Song, S. Huang, C. Li, T. You, K. Long, L. Chen, Y. Chen and X. Ouyang, *Energy Storage Mater.*, 2024, **71**, 103629.

14. Y. Guo, X. Zhu, J. Zhang, T. Zhang, Z. Wang, M. Shan, F. Wang, C. C. Cao, G. Xu and M. Zhu, *Angew. Chem., Int. Ed.*, 2025, **64**, e202422047.

15. S. You, Q. Deng, Z. Wang, Y. Chu, Y. Xu, J. Lu and C. Yang, *Adv. Mater.*, 2024, **36**, 2402245.

16. M. Li, X. Wang, J. Hu, J. Zhu, C. Niu, H. Zhang, C. Li, B. Wu, C. Han and L. Mai, *Angew. Chem., Int. Ed.*, 2023, **62**, e202215552.

17. J. Heo, D. Dong, Z. Wang, F. Chen and C. Wang, *Joule*, 2025, **9**, 101844.

18. P. Xiong, Y. Kang, N. Yao, X. Chen, H. Mao, W.-S. Jang, D. M. Halat, Z.-H. Fu, M.-H. Jung, H. Y. Jeong, Y.-M. Kim, J. A. Reimer, Q. Zhang and H. S. Park, *ACS Energy Lett.*, 2023, **8**, 1613–1625.

19. R. Wang, Q. Ma, L. Zhang, Z. Liu, J. Wan, J. Mao, H. Li, S. Zhang, J. Hao, L. Zhang and C. Zhang, *Adv. Energy Mater.*, 2023, **13**, 2302543.

20. X. Yun, Y. Chen, H. Gao, D. Lu, L. Zuo, P. Gao, G. Zhou, C. Zheng and P. Xiao, *Adv. Energy Mater.*, 2024, **14**, 2304341.

21. R. Zhang, W. K. Pang, J. Vongsvivut, J. A. Yuwono, G. Li, Y. Lyu, Y. Fan, Y. Zhao, S. Zhang, J. Mao, Q. Cai, S. Liu and Z. Guo, *Energy Environ. Sci.*, 2024, **17**, 4569–4581.

22. Q. Ma, R. Gao, Y. Liu, H. Dou, Y. Zheng, T. Or, L. Yang, Q. Li, Q. Cu, R. Feng, Z. Zhang, Y. Nie, B. Ren, D. Luo, X. Wang, A. Yu and Z. Chen, *Adv. Mater.*, 2022, **34**, 2207344.

23. Q. Li, D. Luo, Q. Ma, Z. Zheng, S. Li, Y. Xie, L. Xue, M. Lin, Y. Nie, G. Feng, H. Dou, J. Chen, X. Wang and Z. Chen, *Energy Environ. Sci.*, 2025, **18**, 1489–1501.

24. J. Ren, H. Yan, X. Xu, S. Li and B. Li, *Chem. Eng. J.*, 2024, **498**, 5257.

25. M. Xu, B. Zhang, Y. Sang, D. Luo, R. Gao, Q. Ma, H. Dou and Z. Chen, *Energy Environ. Sci.*, 2024, **17**, 8966–8977.

26. G. Qu, H. Wei, S. Zhao, Y. Yang, X. Zhang, G. Chen, Z. Liu, H. Li and C. Han, *Adv. Mater.*, 2024, **36**, 2400370.

27. Y. Qiu, X. Zheng, R. Zhang, Q. Lin, M. Li, J. Luo, S. Yang, Z. Liu, Q. Wang, Y. Yu and C. Yang, *Adv. Funct. Mater.*, 2024, **34**, 2310825.

28. Z. Wang, J. Diao, J. N. Burrow, Z. W. Brotherton, N. A. Lynd, G. Henkelman and C. B. Mullins, *Adv. Funct. Mater.*, 2024, **34**, 2311271.

29. A. Zhou, H. Wang, X. Hu, Z. Hu, Y. Zhao, B. Zhang, Y. Huang, Y. Cui, Y. Cui, L. Li, F. Wu and R. Chen, *Adv. Funct. Mater.*, 2025, **35**, 2413807.

30. J. Yao, B. Zhang, X. Wang, L. Tao, J. Ji, Z. Wu, X. Liu, J. Li, Y. Gan, J. Zheng, L. Lv, X. Ji, H. Wang, J. Zhang, H. Wang and H. Wan, *Angew. Chem., Int. Ed.*, 2024, **63**, e202409986.

31. T. Liu, C. Lei, H. Wang, J. Li, P. Jiang, X. He and X. Liang, *Adv. Mater.*, 2024, **36**, 2405473.

32. M. Xi, Z. Liu, Z. Tan, Z. Qi, H. Liu, Y. Huang, W. Wang and J. Ding, *Energy Storage Mater.*, 2025, **75**, 104091.

33. Z. Hou, Z. Lu, Q. Chen and B. Zhang, *Energy Storage Mater.*, 2021, **42**, 517–525.

34. Z. Xie, N. Chen, M. Zhang, M. Wang, X. Zheng, S. Liu, R. Luo, L. Song, Y. Meng, Z. Liu, Z. Li and W. Chen, *ACS Energy Lett.*, 2024, **9**, 3380–3390.

35. W. Deng, Z. Xu and X. Wang, *Energy Storage Mater.*, 2022, **52**, 52–60.

36. C. Xie, S. Liu, H. Wu, Q. Zhang, C. Hu, Z. Yang, H. Li, Y. Tang and H. Wang, *Sci. China Mater.*, 2023, **68**, 1531–1539.